Run-up and backwash bore formation from dam-break flow on an inclined plane

MATTEO ANTUONO[1] AND ANDREW J. HOGG[2]†

[1]INSEAN (The Italian Ship Model Basin), US3, Via di Vallerano 139, 00128 Rome, Italy

[2]Centre for Environmental and Geophysical Flows, School of Mathematics, University of Bristol, University Walk, Bristol BS8 1TW, UK

Nonlinear shallow water equations are employed to model the inviscid slumping of fluid along an inclined plane and analytical solutions for the motion are derived using the hodograph transformation to reveal the run-up and the inception of a bore on the backwash. Starting from rest, the fluid slumps along the inclined plane, attaining a maximum run-up, before receding and forming a relatively thin and fast moving backwash. This interacts with the less rapidly moving fluid within the interior to form a bore. The evolution of the bore and the velocity and height fields either side of it are also calculated to reveal that it initially grows in magnitude before diminishing and intersecting with the shoreline. This analytical solution reveals features of the solution, such as the onset of the bore and its growth and decline, previously known only through numerical computation and the method presented here may be applied quite widely to the run-up of other initial distributions of fluid.

1. Introduction

Modelling the dynamics of fluid in the swash zone poses many challenges since the motion is inherently unsteady and turbulent, and has important consequences for sediment transport and beach morphology, as well as for the hydrodynamics of the near-shore region in general (Brocchini & Baldock 2008). For example, previous studies have focused on the run-up of waves along the beach (Shen & Meyer 1963), the associated movement of sediment (Pritchard & Hogg 2005) and the possibility of over-topping coastal structures (Peregrine & Williams 2001). Numerical simulations have attempted to calculate these phenomena, recently employing turbulence closures to resolve the velocity profiles (Zhang & Liu 2008), but more often these are based upon the nonlinear shallow water equations (Brocchini & Dodd 2008). Hibberd & Peregrine (1979) is a particularly notable study in this regard; they were among the first to compute the run-up resulting from the impact of a bore on a uniformly sloping beach. They showed that as the bore collapsed, the shoreline moved essentially ballistically along the beach and at some point during the backwash, a receding bore formed. These observations verified what had been demonstrated for a restricted asymptotic model by Shen & Meyer (1963). Pritchard, Guard & Baldock (2008) have recently extended the analytical treatment to explore the run-up generated by more realistic incoming waves (Guard & Baldock 2007) and to show the inception of the backwash bore.

† Email address for correspondence: a.j.hogg@bris.ac.uk

In this contribution we employ the nonlinear shallow water equations to investigate fluid motion up an inclined planar beach. Our initial conditions are those of dam-break: we study the two-dimensional collapse of an initially motionless reservoir of fluid, generated by the instantaneous removal of the confining dam. This initial condition is of interest in its own right, having a long history of research within a horizontal flume (Ritter 1892; Hogg & Pritchard 2004; Hogg 2006). These flows are readily generated in the laboratory and evolve both spatially and temporally. Although this precise initial condition is different from that considered by Hibberd & Peregrine (1979), or from the idealization of Pritchard *et al.* (2008), the ensuing flow will feature the same important phenomena of wave run-up and the formation of a backwash bore.

In this paper we develop an analytical model of the motion that develops as the dam is removed and the fluid is set into motion. The calculations utilize the hodograph transformation of the governing equations and follows recent progress by Hogg (2006), Pritchard *et al.* (2008) and Antuono, Hogg & Brocchini (2009). We find that the flow develops a bore at some instant and point within the domain during the backwash, and by enforcing conditions that preserve mass and momentum fluxes across the developing discontinuity, we track the evolution of the bore and the velocity and height fields either side of it. We find that the magnitude of the bore, measured in terms of the jump in flow depth, initially grows and then diminishes and that it moves offshore and then onshore before vanishing and intersecting with the retreating shoreline. We believe that this is the first calculation that has analytically tracked the behaviour of the backwash bore and that these results, in addition to being of interest in their own right, yield a challenging test case for algorithms designed to integrate the shallow water equations numerically. Furthermore, this configuration could be readily explored in laboratory experiments, which would reveal the accuracy with which the shallow water equations capture the true fluid motions; however, we have been unable to find any published results in this configuration. The paper is structured as follows. First, we formulate the problem and introduce the dimensionless equations and hodograph transformation (§2). We construct the results, first focusing on the motion before the bore forms (§3) and then constructing the evolution of the bore and the flow fields either side of it (§4). Finally, we summarize the results (§5).

2. Governing equations and the hodograph transformation

We consider motion up an inclined planar surface when fluid is instantaneously released from a state of rest within a reservoir behind a dam. The two-dimensional motion that ensues is assumed to be predominantly parallel to the underlying boundary, so that fluid accelerations perpendicular to the plane are negligible and the pressure adopts a hydrostatic distribution. We adopt x and z coordinates axes that are parallel and perpendicular to the plane, respectively, with the origin located at the base of the dam; the inclination of the plane is denoted by θ. Then the dimensionless shallow water equations that govern the evolution of the depth of the flow, $d(x, t)$ and its velocity, $u(x, t)$ are given by (see Peregrine 1972)

$$\frac{\partial d}{\partial t} + \frac{\partial}{\partial x}(ud) = 0 \quad \text{and} \quad \frac{\partial u}{\partial t} + u\frac{\partial u}{\partial x} + \frac{\partial d}{\partial x} = -1. \tag{2.1}$$

In these equations, length scales parallel and perpendicular to the plane have been rendered dimensionless with respect to $h_0/\tan\theta$ and h_0, respectively, where h_0 denotes the height of fluid immediately behind the dam. Times are non-dimensionalized

by $(h_0 \cos\theta/g)^{1/2}/\sin\theta$, where g denotes gravitational acceleration. With these dimensional scales, we find that there is one remaining dimensionless parameter, $L \equiv \tan\theta L^*/h_0$, that essentially measures the length of the reservoir (L^*). The initial conditions are that $u(x, t) = 0$ and

$$d = \begin{cases} 1 - x, & -L \leqslant x \leqslant 0, \\ 0, & x > 0, \end{cases} \qquad (2.2)$$

while at the end of the reservoir, we impose the condition of no flow, $u(-L, t) = 0$. The shallow-layer model (2.1) neglects hydraulic resistance, an assumption that may become invalid close to the front of the motion where the fluid depths become very small (see Hogg & Pritchard 2004). However dissipation is implicitly included through the development of the backwash bore.

The governing equations (2.1) can be rewritten in characteristic form as follows:

$$\alpha \equiv u + t + 2c = \text{constant} \quad \text{along curves such that} \quad \dot{x} = u + c, \qquad (2.3)$$
$$\beta \equiv u + t - 2c = \text{constant} \quad \text{along curves such that} \quad \dot{x} = u - c, \qquad (2.4)$$

where $c = \sqrt{d}$, where a dot denotes differentiation with respect to time. Using α and β as independent variables instead of x and t (the hodograph transformation), we obtain the following relations:

$$u = \frac{\alpha + \beta}{2} - t, \quad c = \frac{\alpha - \beta}{4}, \qquad (2.5)$$

while (2.3) and (2.4) become

$$\frac{\partial x}{\partial \beta} = \left(\frac{3\alpha + \beta}{4} - t\right)\frac{\partial t}{\partial \beta} \quad \text{along curves such that} \quad \alpha = \text{constant}, \qquad (2.6)$$

$$\frac{\partial x}{\partial \alpha} = \left(\frac{\alpha + 3\beta}{4} - t\right)\frac{\partial t}{\partial \alpha} \quad \text{along curves such that} \quad \beta = \text{constant}. \qquad (2.7)$$

Combining (2.6) and (2.7), we find

$$\frac{\partial^2 t}{\partial\alpha\,\partial\beta} = \frac{3}{2(\alpha - \beta)}\left(\frac{\partial t}{\partial\alpha} - \frac{\partial t}{\partial\beta}\right). \qquad (2.8)$$

The hodograph transformation remains invertible provided the Jacobian of the transformation J remains finite and non-vanishing. By using (2.6) and (2.7), it is possible to show that

$$J \equiv \frac{\partial t}{\partial\alpha}\frac{\partial x}{\partial\beta} - \frac{\partial t}{\partial\beta}\frac{\partial x}{\partial\alpha} = 2c\,\frac{\partial t}{\partial\alpha}\frac{\partial t}{\partial\beta}. \qquad (2.9)$$

3. The dam-break problem

We study the motion that ensues when the fluid is instantaneously released. To solve this problem, we use the theoretical scheme described in Hogg (2006), which employs the linear differential form given by $\omega = -V\,\mathrm{d}a + U\,\mathrm{d}b$, in which

$$V = \frac{3t\,B}{2(a-b)} + \frac{B}{2}\frac{\partial t}{\partial a} - \frac{t}{2}\frac{\partial B}{\partial a} \quad \text{and} \quad U = -\frac{3t\,B}{2(a-b)} + \frac{B}{2}\frac{\partial t}{\partial b} - \frac{t}{2}\frac{\partial B}{\partial b}. \qquad (3.1)$$

In these expressions $B = B(a, b; \alpha, \beta)$ is the Riemann function that satisfies the partial differential equation adjoint to (2.8), which is given by

$$\frac{\partial^2 B}{\partial a \partial b} + \frac{3}{2(a-b)}\left(\frac{\partial B}{\partial a} - \frac{\partial B}{\partial b}\right) - \frac{3 B}{(a-b)^2} = 0, \tag{3.2}$$

subject to the boundary conditions

$$\frac{\partial B}{\partial b} = \frac{-3 B}{2(a-b)} \text{ along } a = \alpha, \quad \frac{\partial B}{\partial a} = \frac{3 B}{2(a-b)} \text{ along } b = \beta \quad \text{and} \quad B(\alpha, \beta; \alpha, \beta) = 1. \tag{3.3}$$

In this case, the Riemann function is given by Garabedian (1986):

$$B(a, b; \alpha, \beta) = \frac{(a-b)^3}{(a-\beta)^{3/2}(\alpha-b)^{3/2}} F\left[\frac{3}{2}, \frac{3}{2}; 1; \frac{(a-\alpha)(\beta-b)}{(a-\beta)(\alpha-b)}\right], \tag{3.4}$$

where F is the hypergeometric function. According to the Riemann method, a function $t(\alpha, \beta)$ satisfies (2.8) if and only if the linear differential form ω is exact, that is, if for all regular domains D in the (α, β) plane, we require

$$\int_{\partial D} \omega = 0, \tag{3.5}$$

where ∂D represents the boundary of D.

   Now we are in a position to solve the problem. When the right rigid wall is removed $(t = 0^+)$, a front curve $x = x_N(t)$ is generated, which is defined as the curve separating the wet and dry parts of the sloping plane. This interface is advected with the fluid velocity and so satisfies the kinematic condition $dx_N/dt = u$. Furthermore, at the front the height vanishes $(c = 0)$ and so we can rewrite the kinematic condition as $\dot{x}_N = \alpha - t$. Note also that along the front curve $\alpha = \beta$.

   The last equality implies that, similarly to the dam break on a horizontal plane, a rarefaction fan is generated just after the right rigid wall is removed. Indeed, at $t = 0^-$ and $x = 0$, the values of the characteristic variables are $\alpha = 2$ and $\beta = -2$. When the right rigid wall is removed $(t = 0^+)$, a front curve is generated along which $\beta = \alpha = 2$. This means that at $t = 0^+$ and $x = 0$ the Riemann invariant β has to vary continuously between -2 and 2 and consequently a fan of β-characteristic curves is generated at $x = 0$. However, in contrast to the solution for the horizontal plane, such a fan is not associated with a simple wave region, because the adjoining region associated with the initial conditions does not feature constant values of the characteristic variables, α and β.

3.1. *Region U_1*

Within U_1 the characteristics originate from $-L \leqslant x < 0$ and because the initial state is one of no flow, then $\beta(x, 0) = -\alpha(x, 0)$ and $2 \leqslant \alpha(x, 0) \leqslant 2(1 + L)^{1/2}$. The region is bounded by the rear wall at $x = -L$ and the rearmost β-characteristic from the origin (denoted by δ_1 in figure 1). Throughout U_1 we have $u = 0$, $d = 1 - x$ and the α- and β-characteristic curves (hereinafter denoted by the symbols γ and δ respectively) are given by

$$\gamma: \quad x(t) = 1 - \frac{(t - 2\sqrt{1 - x_0})^2}{4}, \quad \alpha = t + 2\sqrt{1 - x},$$

$$\delta: \quad x(t) = 1 - \frac{(t + 2\sqrt{1 - x_0})^2}{4}, \quad \beta = t - 2\sqrt{1 - x},$$
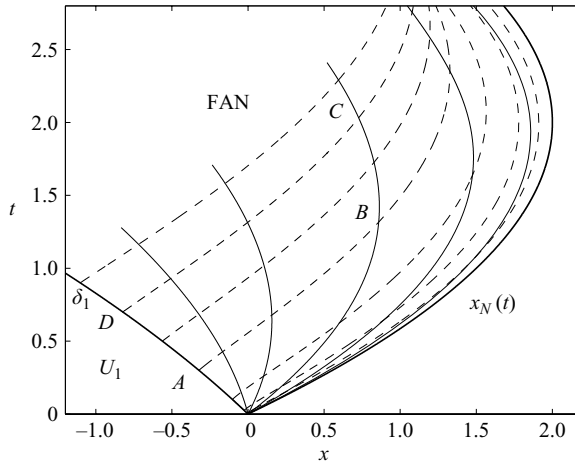
FIGURE 1. Characteristics in the (x, t) plane, including the region U_1 and the fan, generated from $x = 0$ (α-characteristics are plotted with a dashed line and β-characteristics with a solid line). Also depicted is the integration contour $ABCD$ and the bounding characteristic δ_1 between U_1 and the fan.

with $-L \leqslant x_0 \leqslant 0$. The characteristic curve on which $\beta = -2$ (curve δ_1) is of fundamental importance for the analysis that follows because it represents the rearmost boundary of the fan. Using (2.3) and (2.4), it is straightforward to establish that δ_1 is given by

$$t(\alpha, -2) = \frac{\alpha}{2} - 1 \quad \text{and} \quad x(\alpha, -2) = 1 - \frac{(\alpha + 2)^2}{16}. \tag{3.6}$$

Thus we deduce that the δ_1 characteristic intersects the rear wall at $t = t_w \equiv 2\sqrt{1 + L} - 2$, when $\alpha = \alpha_w \equiv 4\sqrt{1 + L} - 2$. Thereafter a forward propagating characteristic is generated from $(0, t_w)$ and this modifies the solution within the fan; this means that the solution developed below is appropriate only for $2 < \alpha < \alpha_w$. However it is possible to construct the solution affected by the no-flow condition at the back of the lock using Riemann's method (see Kerswell 2005; Antuono *et al.* 2009 for details), but this is not the focus of the current study.

3.2. *The fan region*

We construct the solution using Riemann's method applied to the region $ABCD$ bounded by characteristic curves and depicted in figure 1. The curve AD is made by the β-characteristic δ_1 while the curve BC is a β-characteristic inside the fan. The curves AB and CD are α-characteristics within the fan. The coordinates of the points A, B, C, D in the hodograph plane are given by

$$A = (\alpha_1, -2), \quad B = (\alpha_1, \beta), \quad C = (\alpha, \beta), \quad D = (\alpha, -2), \tag{3.7}$$

where α_1 is the value carried by the α-characteristic curve along the line AB. Now, we apply the Riemann construction in (3.5) with $B = B(a, b; \alpha, \beta)$. We find

$$0 = \int_{ABCD} \omega = \int_{-2}^{\beta} U|_{a=\alpha_1} \, \mathrm{d}b - \int_{\alpha_1}^{\alpha} V|_{b=\beta} \, \mathrm{d}a + \int_{\beta}^{-2} U|_{a=\alpha} \, \mathrm{d}b - \int_{\alpha}^{\alpha_1} V|_{b=-2} \, \mathrm{d}a. \tag{3.8}$$

We now consider the limit $\alpha_1 \to 2$ and use the conditions that $t(2, \beta) = x(2, \beta) = 0$ to show that

$$\lim_{\alpha_1 \to 2} \int_{AB} \omega = 0. \tag{3.9}$$

The second integral of (3.8) may be computed using the boundary condition (3.3), integration by parts and subsequent evaluation as $\alpha_1 \to 2$, to give

$$\lim_{\alpha_1 \to 2} \int_{BC} \omega = - \lim_{\alpha_1 \to 2} \frac{1}{2} \left(t(\alpha, \beta) - B(\alpha_1, \beta; \alpha, \beta) t(\alpha_1, \beta) \right) = -\frac{t(\alpha, \beta)}{2}. \tag{3.10}$$

The third integral of (3.8) is also evaluated using the boundary condition (3.3) and integration by parts to yield

$$\int_{CD} \omega = \frac{1}{2} \left(B(\alpha, -2; \alpha, \beta) t(\alpha, -2) - t(\alpha, \beta) \right) = \left(\frac{\alpha + 2}{\alpha - \beta} \right)^{3/2} \frac{t(\alpha, -2)}{2} - \frac{t(\alpha, \beta)}{2}. \tag{3.11}$$

This expression includes a contribution from the curve δ_1, along which $t(\alpha, -2)$ is given by (3.6). This also permits evaluation of the final contribution in (3.8)

$$\int_{DA} \omega = \frac{B(\alpha, -2; \alpha, \beta) t(\alpha, -2)}{2} - \int_\alpha^2 \left(t \left[\frac{3B}{2(a-b)} - \frac{\partial B}{\partial a} \right] \right) \Bigg|_{b=-2} da. \tag{3.12}$$

Collecting together all the contributions and one further integration by parts yields the following result for the time field within the fan

$$t(\alpha, \beta) = \int_2^\alpha B(a, -2; \alpha, \beta) \left[\frac{3(a-2)}{4(a+2)} + \frac{1}{2} \right] da. \tag{3.13}$$

We note that this expression is a special case of the wave-like solutions derived by Pritchard *et al.* (2008). Given this parametric expression for the time t as a function of the hodograph variables α and β, it is straightforward to find $x(\alpha, \beta)$ by integrating the equation along characteristic curves (2.6) and (2.7). Then using the conditions $t(2, \beta) = 0$ and $x(2, \beta) = 0$, we obtain

$$x(\alpha, \beta) = \left(\frac{\alpha + 3\beta}{4} - \frac{t}{2} \right) t(\alpha, \beta) - \frac{1}{4} \int_2^\alpha t(a, \beta) \, da. \tag{3.14}$$

Figure 1 shows the α- and β-characteristic curves inside the fan region. It is evident that the two families of characteristic curves coincide when $\alpha \to 2^+$ and $\beta \to 2^-$, that is, as the front is approached.

The point $(\alpha, \beta) = (2, 2)$ is a singular point for the solution in the fan region and therefore it is not possible to get an explicit expression for $x_N(t)$ from (3.13). This is to be anticipated, because the Jacobian of the hodograph transformation vanishes when the depth of the fluid vanishes (see (2.9)). However the position of the front may be readily calculated by noting that $\alpha = \beta = 2$ and consequently $\dot{x}_N = \alpha - t = 2 - t$. Thus we find that

$$x_N(t) = 2t - \frac{t^2}{2}. \tag{3.15}$$

Figure 1 clearly shows the analytical solution given by (3.13) matching with the front curve in (3.15). From (3.15), we note that maximum run-up occurs at $t = 2$ and that $x_N(2) = 2$. For $t > 2$ the run-down of the front wave starts. Profiles of the velocity and depth of fluid are plotted in figure 2 at various times from initiation until the solution breaks down, including the time of maximum run-up. It is noteworthy that non-vanishing offshore velocity develops at some interior location before maximum
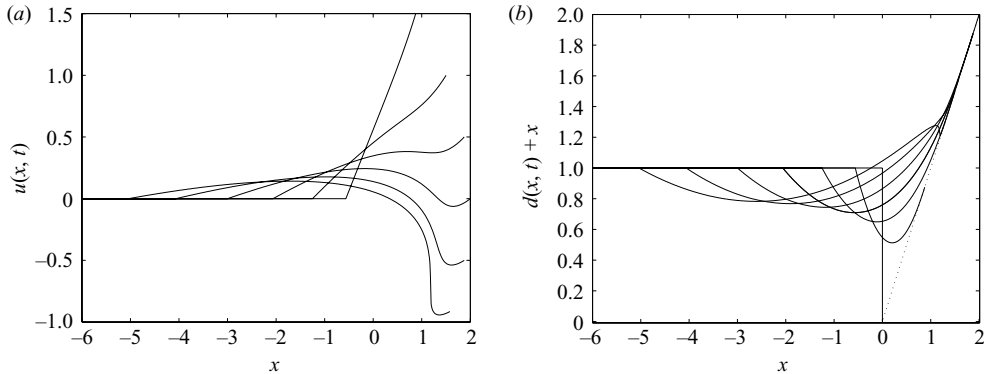
FIGURE 2. The profiles of the velocity $u(x,t)$ and the free surface elevation of fluid $d(x,t)+x$ at $t = 0, 0.5, 1.0.1.5, 2.0, 2.5, 2.916$. At the latest time, the solution first develops infinite gradients and thereafter an internal shock develops. In (b) the dotted line depicts the underlying rigid boundary and the depth of the fluid vanishes when $d(x,t)+x$ intersects this line.

run-up is attained, as is often found in nonlinear shallow water models of swash (Shen & Meyer 1963; Pritchard *et al.* 2008).

3.3. *Breakdown of solution*

The hodograph transformation becomes non-invertible whenever the Jacobian J vanishes or becomes unbounded. For this solution (3.13), the earliest time at which the Jacobian vanishes is given by the conditions

$$\frac{\partial t}{\partial \alpha} = 0 \quad \text{and} \quad \frac{\partial^2 t}{\partial \alpha^2} = 0, \tag{3.16}$$

which corresponds to the first instance at which α-characteristics intersect. The conditions (3.16) are satisfied at $(\alpha, \beta) \equiv (\alpha_*, \beta_*) = (2.622, 1.791)$, while $t(\alpha_*, \beta_*) \equiv t_* = 2.916$ and $x(\alpha_*, \beta_*) \equiv x_* = 1.181$. Thereafter it is no longer appropriate to describe the entire domain by (3.13), but rather a bore must be inserted to join the seaward and landward regions and render the multivalued region as single-valued. However the solution (3.13) does remain appropriate for β-characteristics with $\beta < \beta_*$ and the limiting $\beta = \beta_*$ characteristic bounds the multivalued region. The profiles of the height and velocity fields are plotted in figure 2 at the instant when the solution breaks down ($u(x, t_*)$ and $d(x, t_*)$).

4. Shock solution

The multivalued solution that emerges for $t > t_*$ is resolved by introducing a bore across which the velocity and height fields are discontinuous. This implies that the hodograph variables are also discontinuous, and thus the bore opens up a 'tear' in the hodograph plane (cf. Hogg 2006). The solutions either side of the discontinuity are related by jump conditions that express conservation of mass and momentum. Thus denoting the shock speed by s, we may write these jump conditions as

$$[ud] = s\,[d] \quad \text{and} \quad \left[u^2 d + \frac{1}{2} d^2\right] = s\,[ud], \tag{4.1}$$

where $[\ldots]$ represents the change in value between the landward and seaward sides of the shock, henceforth denoted by the subscripts 1 and 2, respectively. We note that

some care must be taken when employing the nonlinear shallow water equations to model the motion close to bores, because there are non-negligible vertical accelerations that may render the pressure no longer hydrostatic. However these shock conditions (4.1) preserve the mass and momentum fluxes, while leading implicitly to dissipation across the shock. They are the traditional mathematical representations of the steep-fronted fluid motion associated with bores (see e.g. Hibberd & Peregrine 1979). We re-write (4.1) in terms of the hodograph variables: at this stage, following Antuono *et al.* (2009), it is convenient to introduce $\lambda = \alpha + \beta$ and $\sigma = \alpha - \beta$ as this permits the shock equations to be solved analytically. However tracking the shocks under consideration here is more complicated than those treated by Antuono *et al.* (2009): here the flow both sides of the shock are evolving temporally and spatially, whereas there was a spatially uniform state on one side of the shocks in Antuono *et al.* (2009), thus allowing the characteristic variables to be determined straightaway. We find that

$$\lambda_2 = \lambda_1 - \frac{\left(\sigma_1^2 - \sigma_2^2\right)}{4\sigma_1\sigma_2}\left(2\left(\sigma_1^2 + \sigma_2^2\right)\right)^{1/2}. \tag{4.2}$$

In this expression, the negative branch of the square root has been chosen, because the jump results in an increase of height ($\sigma_2 > \sigma_1$) and a reduction of seaward velocity ($|\lambda_1| > |\lambda_2|$). The shock speed is given by

$$s + t = \frac{\lambda_1}{2} + \frac{\sigma_2}{8\sigma_1}\left(2\left(\sigma_1^2 + \sigma_2^2\right)\right)^{1/2}. \tag{4.3}$$

The location of the shock is written parametrically as $(x_s(\alpha), t_s(\alpha))$, where α denotes the characteristic value on the landward side. The β-characteristic value at the shock on the landward side is denoted by $\beta(\alpha)$, while the characteristic values on the seaward side are denoted by $\alpha_s(\alpha)$ and $\beta_s(\alpha)$. The parameter α varies between α_* and 2. The evolution of the shock is parametrically expressed by

$$\frac{\mathrm{d}x_s}{\mathrm{d}\alpha} = s\frac{\mathrm{d}t_s}{\mathrm{d}\alpha}. \tag{4.4}$$

Initially at the inception of the shock $\sigma_2 \to \sigma_1$ and so from (4.3) $s \to u + \sqrt{h}$. Thus the shock is initially tangent to the characteristic on which $\alpha = \alpha_*$, confirming our implicit assumption that there is no fan of β-characteristics generated from (α_*, β_*).

On the seaward side of the shock, we may view the shock curve as a function of α_s and β_s. Thus

$$\frac{\mathrm{d}x_s}{\mathrm{d}\alpha} = \frac{\mathrm{d}\alpha_s}{\mathrm{d}\alpha}\frac{\partial x}{\partial \alpha} + \frac{\mathrm{d}\beta_s}{\mathrm{d}\alpha}\frac{\partial x}{\partial \beta}. \tag{4.5}$$

Then using (2.6) and (2.7), we may write this as

$$\frac{\mathrm{d}x_s}{\mathrm{d}\alpha} = \left(\frac{\alpha + \beta}{2} - t_s\right)\frac{\mathrm{d}t_s}{\mathrm{d}\alpha} + \frac{\beta_s - \alpha_s}{4}\left(\frac{\mathrm{d}\alpha_s}{\mathrm{d}\alpha}\frac{\partial t_s}{\partial \alpha} - \frac{\mathrm{d}\beta_s}{\mathrm{d}\alpha}\frac{\partial t_s}{\partial \beta}\right). \tag{4.6}$$

Thus we deduce that

$$\frac{\mathrm{d}t_s}{\mathrm{d}\alpha}\left(s + t_s - \frac{\alpha_s + \beta_s}{2}\right) = \frac{\beta_s - \alpha_s}{4}\left(\frac{\mathrm{d}\alpha_s}{\mathrm{d}\alpha}\frac{\partial t_s}{\partial \alpha} - \frac{\mathrm{d}\beta_s}{\mathrm{d}\alpha}\frac{\partial t_s}{\partial \beta}\right), \tag{4.7}$$

and this identity will be used to simplify the analysis that follows.

The task is now to calculate the trajectory of the shock curve in the hodograph plane; that is, we must calculate $\beta(\alpha)$, $\beta_s(\alpha)$ and $\alpha_s(\alpha)$. At each value of α we enforce continuity of x and t across the shock and the remaining shock condition (4.2). Given
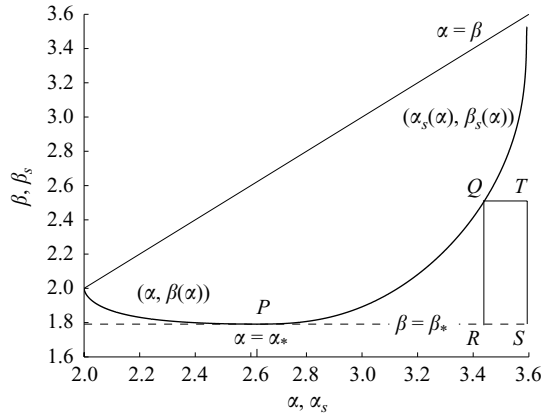
FIGURE 3. The hodograph plane and the tear that develops across the developing discontinuity. The onshore side of the shock corresponds to the curve $(\alpha, \beta(\alpha))$, while the offshore side corresponds to the curve $(\alpha_s(\alpha), \beta_s(\alpha))$. Both curves originate from the point at which the Jacobian of the hodograph transformation first becomes non-invertible. Also depicted are the integration contours PQR and $PQTS$.

$t(\alpha_s, \beta_s)$, it is straightforward to find $x(\alpha_s, \beta_s)$ using (4.4) and (4.3) – and $t(\alpha_s, \beta_s)$ is determined using Riemann's method in the hodograph plane (3.5), as described in what follows.

We integrate (3.5) around a closed contour PQR, where

$$P = (\alpha_*, \beta_*), \quad Q = (\alpha_s(\alpha), \beta_s(\alpha)) \quad \text{and} \quad R = (\alpha_s(\alpha), \beta_*)) \tag{4.8}$$

(see figure 3). On QR and RP, the contributions, denoted by I_1 and I_2, respectively, are readily evaluated using integration by parts because these are straight lines in the hodograph plane. Thus we find that

$$I_1 = \int_{\beta_s}^{\beta_*} U \, \mathrm{d}b = \frac{1}{2} \left(t(\alpha_s, \beta_*) - B(\alpha_s, \beta_s; \alpha_s, \beta_*) t(\alpha_s, \beta_s) \right) \tag{4.9}$$

$$\text{and} \quad I_2 = \int_{\alpha_s}^{\alpha_*} -V \, \mathrm{d}a = \frac{1}{2} \left(t(\alpha_*, \beta_*) - B(\alpha_*, \beta_*; \alpha_s, \beta_*) t_* \right). \tag{4.10}$$

However the contribution from the curved segment PQ, denoted by I_3, is more difficult to evaluate. The segment is given parametrically by $a = \alpha_s(\alpha)$ and $b = \beta_s(\alpha)$ and the form of the curve is to be determined as part of the solution. We find that

$$
\begin{aligned}
I_3 &= \int_{\alpha_*}^{\alpha} \left(-V \frac{\mathrm{d}a_s}{\mathrm{d}\alpha} + U \frac{\mathrm{d}b_s}{\mathrm{d}\alpha} \right) \mathrm{d}\alpha, \\
&= \int_{\alpha_*}^{\alpha} \frac{-3 t_s B}{2(a_s - b_s)} \left(\frac{\mathrm{d}a_s}{\mathrm{d}\alpha} + \frac{\mathrm{d}b_s}{\mathrm{d}\alpha} \right) + \frac{t_s}{2} \left(\frac{\partial B}{\partial a} \frac{\mathrm{d}a_s}{\mathrm{d}\alpha} - \frac{\partial B}{\partial b} \frac{\mathrm{d}b_s}{\mathrm{d}\alpha} \right) \\
&\quad - \frac{B}{2} \left(\frac{\partial t_s}{\partial a} \frac{\mathrm{d}a_s}{\mathrm{d}\alpha} - \frac{\partial t_s}{\partial b} \frac{\mathrm{d}b_s}{\mathrm{d}\alpha} \right) \mathrm{d}\alpha,
\end{aligned}
\tag{4.11}
$$

where a_s and b_s are parametric representations of the curve PQ, $t_s \equiv t(a_s, b_s)$, and in this integrand $B \equiv B(a_s, b_s; \alpha_s, \beta_*)$ and likewise for the derivatives of B. Finally, we use (4.7) to simplify this expression, which replaces the derivatives of t normal to the

curve by ones tangent to it. Thus we find that

$$I_3 = \int_{\alpha_*}^{\alpha} \frac{-3t_s B}{2(a_s - b_s)} \left(\frac{\mathrm{d}a_s}{\mathrm{d}\alpha} + \frac{\mathrm{d}b_s}{\mathrm{d}\alpha} \right) + \frac{t_s}{2} \left(\frac{\partial B}{\partial a} \frac{\mathrm{d}a_s}{\mathrm{d}\alpha} - \frac{\partial B}{\partial b} \frac{\mathrm{d}b_s}{\mathrm{d}\alpha} \right)$$

$$+ \frac{2B}{a_s - b_s} \left(s + t_s - \frac{(a_s + b_s)}{2} \right) \frac{\mathrm{d}t_s}{\mathrm{d}\alpha} \, \mathrm{d}\alpha. \quad (4.12)$$

Substituting for the Riemann function B, we derive the following integral equation for the variation of the time along the curve PA,

$$t(\alpha_s, \beta_s) = 2 \left(\frac{\alpha_s - \beta_*}{\alpha_s - \beta_s} \right)^{3/2} t(\alpha_s, \beta_*) - \left(\frac{\alpha_* - \beta_*}{\alpha_s - \beta_s} \right)^{3/2} t_* + 2 \left(\frac{\alpha_s - \beta*}{\alpha_s - \beta_s} \right)^{3/2} I_3. \quad (4.13)$$

This integral equation is for the time, $t(\alpha_s, \beta_s)$, on the seaward side of the shock. However by continuity this is the same as the time on the landward side, $t(\alpha, \beta(\alpha))$, which is known. Thus (4.13) can be regarded as an equation linking the parametric form of the shock curves in the hodograph plane on its landward $(\alpha, \beta(\alpha))$ and seaward sides $(\alpha_s(\alpha), \beta_s(\alpha))$.

Our numerical strategy for solving these equations is as follows: for each value of α, we make an initial guess for the values of $\alpha_s(\alpha)$ and $\beta(\alpha)$. The jump condition, (4.2), then determines $\beta_s(\alpha)$ and the shock speed $s(\alpha)$. We evaluate $t(\alpha_s, \beta_s)$ and $x(\alpha_s, \beta_s)$ from the integral equation and the evolution of the shock speed and iteratively adjust our initial guess until we attain a converged solution. We tackle this for discrete, decreasing values of α in the range $2 < \alpha \leqslant \alpha_*$.

There are some difficulties with this numerical strategy. First, it is necessary to initiate the calculations with a good initial guess for α_s and β. To this end we develop the following power series expansions for α_s, β_s and β as functions of $\epsilon \equiv \alpha - \alpha_* \ll 1$. By substituting these into the governing equation and by balancing in powers of ϵ, we find that to leading order

$$\alpha_s = \alpha_* - \epsilon + \cdots \quad \text{and} \quad \left. \begin{array}{l} \beta_s \\ \beta \end{array} \right\} = \beta_* + \epsilon^2 \frac{(\alpha_* - \beta_*)}{9} \frac{\partial^3 t}{\partial \alpha^3} \left(\frac{\partial t}{\partial \beta} \right)^{-1} + \cdots, \quad (4.14)$$

where the derivatives are evaluated at $(\alpha, \beta) = (\alpha_*, \beta_*)$. Further difficulties are encountered as the moving shoreline approaches the shock. In this limit, $\alpha \to 2$, $\beta \to 2$ and $\alpha_s - \beta_s \to 0$ and thus the expression (4.13) contains divergent terms that can strongly influence the computations. We analyse the behaviour in the regime $0 < \tilde{\epsilon} \equiv \alpha - 2 \ll 1$ to deduce the dependence of α_s, β_s and β upon $\tilde{\epsilon}$. First, we note that from (3.13),

$$\left. \frac{\partial t}{\partial \alpha} \right|_{\alpha=2} = \frac{4}{(2 - \beta)^{3/2}}. \quad (4.15)$$

Thus if t is to remain bounded and non-vanishing in the regime $\tilde{\epsilon} \ll 1$, we require that $2 - \beta = O(\tilde{\epsilon}^{2/3})$. Then from the jump condition (4.2), it is possible for the velocity to change across the discontinuity if $\sigma_2^2/\sigma_1 = O(1)$ as $\sigma_1 \to 0$ and $\sigma_2 \to 0$. Thus $\alpha_s - \beta_s = O(\tilde{\epsilon}^{1/3})$. This in turn implies that the shock speed $s = u_2$ to leading order. These dependencies on $\tilde{\epsilon}$ imply that relatively rapid variation is to be anticipated as $\tilde{\epsilon} \to 0$. Thus we evaluate the shock at an irregular spacing of α, clustering values towards $\alpha = 2$ to resolve the rapid variation in that region. For the results presented below we employed $\alpha_i = 2 + (1 - i/N)^3(\alpha_* - 2)$ with $N = 4000$ and the results were accurate to 10^{-3}, checked by doubling the number of points. The trajectory of the shock in the (x, t) plane and the tear that it induces in the hodograph plane are
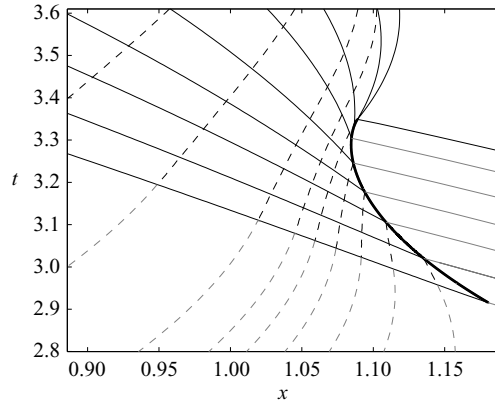
FIGURE 4. The characteristic plane and the shock curve (x_s, t_s) (thick line), depicting α-characteristics (dashed lines) and β-characteristics (solid lines) within the region affected by the presence of the shock. The characteristics curves outside of this region are plotted with faint lines.
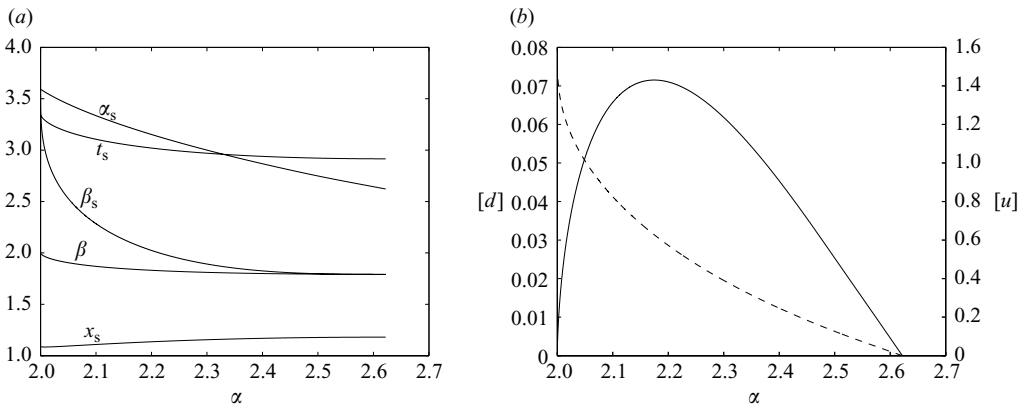

FIGURE 5. (*a*) The shock variables $(\alpha_s, \beta_s, \beta, t_s, x_s)$ and (*b*) the jump of the depth of the fluid (solid line) and the velocity (dashed line) as s functions of the characteristic value α on the shoreward side of the shock. Note that $2 < \alpha < \alpha_*$.

plotted in figures 3 and 4, while the quantities that describe the shock and its location $(\alpha_s, \beta_s, \beta, t_s, x_s)$ are plotted as functions of α in figure 5. We note a progressive growth in the size of the discontinuities across the shock, followed by a subsequent diminishing as the shoreline is approached. (See figure 5*b* in which the magnitudes of the jumps in velocity and depth are plotted as functions of α.) Notably the shock speed becomes positive (onshore) for $2 < \alpha < 2.008$ and the shock moves onshore for a short period before intersecting with the shoreline at $t \equiv t_m = 3.349$, $x \equiv x_m = 1.089$ and $\alpha_s = \beta_s \equiv \alpha_m = 3.59$. Thereafter the shoreline is governed locally by $\mathrm{d}x_N/\mathrm{d}t = \alpha_m - t$. However this is not the complete solution as the shoreline becomes an envelope of α-characteristics (cf. Hibberd & Peregrine 1979).

The solution seaward of the shock may be readily evaluated using Riemann's method once the trajectory of the shock in the hodograph plane is known. In this case we integrate around the closed contour $PQTS$, where P and Q denote locations at the start of and on the shock trajectory, respectively (as defined above and plotted
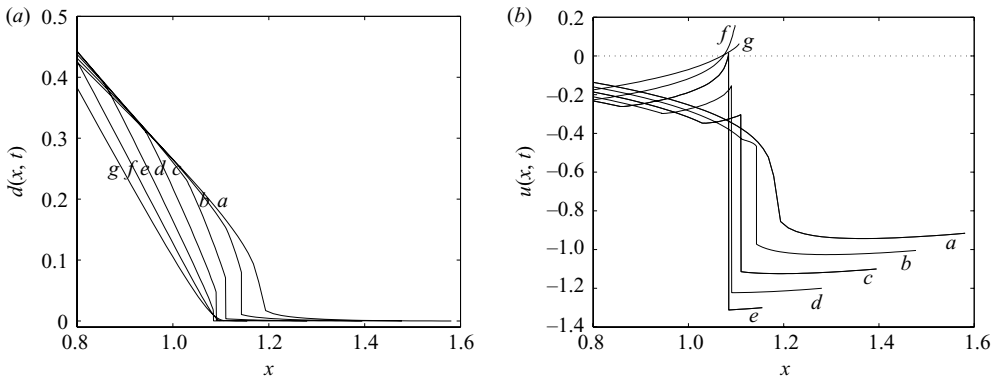
FIGURE 6. (a) The depth of the fluid and (b) the velocity of the flow as functions of distance at times $t = t_*$, 3.0, 3.1, 3.2, 3.3, 3.4, 3.5 (labelled a–g). Note that the shock forms at $t = t_* \equiv 2.916$ and that it has dissipated in the profiles for $t = 3.4$, 3.5.

in figure 3) and the other points form straight line segments in the hodograph plane with $T = (\tilde{\alpha}, \beta_s)$ and $S = (\tilde{\alpha}, \beta_*)$. Then summing the contributions from each of the segments, we deduce that

$$
\begin{aligned}
t(\tilde{\alpha}, \beta_s) = {} & \left(\frac{\tilde{\alpha} - \beta_*}{\tilde{\alpha} - \beta_s} \right)^{3/2} t(\tilde{\alpha}, \beta_*) + \frac{1}{2} \left(\frac{\tilde{\alpha} - \beta_*}{\tilde{\alpha} - \beta_s} \right)^{3/2} B(\alpha_s, \beta_s; \tilde{\alpha}, \beta_*) t(\alpha_s, \beta_s) \\
& - \frac{1}{2} \left(\frac{\alpha_* - \beta_*}{\tilde{\alpha} - \beta_s} \right)^{3/2} t_* + \left(\frac{\tilde{\alpha} - \beta_*}{\tilde{\alpha} - \beta_s} \right)^{3/2} \tilde{I}_3 + \left(\frac{\tilde{\alpha} - \beta_*}{\tilde{\alpha} - \beta_s} \right)^{3/2} \\
& \times \int_{\alpha_s}^{\tilde{\alpha}} t(a, \beta_s) \left(\frac{\partial B}{\partial a} - \frac{3B}{2(a - \beta_s)} \right) \mathrm{d}a,
\end{aligned} \tag{4.16}
$$

where the final integral is evaluated along $b = \beta_s$ and $\tilde{I}_3$ is equal to I_3 with the Riemann function now evaluated as $B = B(a_s, b_s, \tilde{\alpha}, \beta_*)$ and likewise for its derivatives. The position $x(\tilde{\alpha}, \beta_s)$ is computed by integrating (2.7) along the $\beta = \beta_s$ characteristic.

Armed with these expressions for the solution offshore of the shock, we may now compute the complete solution. In figure 4, we plot the α- and β-characteristic curves, noting how they intersect with the shock. In figure 6 we plot snapshots of the velocity and depth profiles in the vicinity of the shock. These plots depict the variation of u and d as the shock grows and diminishes and in the aftermath of its intersection with the shoreline. The positions at which the gradients of u and d are discontinuous in figure 6 correspond to the $\beta = \beta_*$ characteristic; shoreward of this point the solution is affected by the shock, whereas seaward it is unaffected.

The fluid motion near the retreating front is relatively thin, but exhibits a relatively rapid offshore velocity (see figures 2 and 6). This offshore flow encounters much deeper and more slowly moving fluid and it is this interaction that generates the landward-facing bore. After the bore formation, it grows as more offshore moving fluid is fed into it, but eventually this offshore flux becomes sufficiently small and the bore collapses shoreward, thus diminishing in magnitude and generating a weak onshore motion. This sequence of dynamical phenomena is similar to that found by Hibberd & Peregrine (1979) in their study of run-up and backwash bore formation from a uniform bore approaching a planar beach. Their insights into these physical features were drawn from their numerical computations, which integrated the nonlinear shallow water equations. In the current study of the slumping of fluid from dam-break

initial conditions, however, we have been able to track the onset and evolution of the bore using these quasi-analytical techniques that are based upon the hodograph transformation of the governing equations.

Finally, we may evaluate the magnitude of L such that the impermeable back wall of the tank does not influence the evolution of the shock. The forward propagating characteristic from the wall has $\alpha = \alpha_w$. Thus there are two critical values of L, given by $L_1 = -1 + (\alpha_m + 2)^2/16$ and $L_2 = -1 + (\alpha_* + 2)^2/16$. If $L > L_1$ then the rear wall does not affect the formation and evolution of the shock. If $L_1 > L > L_2$ then the formation of the shock is not affected by the back wall, but at some point during its development, it intersects with the α-characteristic emanating from the rear wall and the subsequent evolution is modified. However if $L_2 > L$ then the presence of the rear wall also modifies the initial inception of the shock.

5. Summary and conclusions

In this study we have developed a new analytical solution to the governing equations that reveals the two-dimensional run-up of fluid on a planar beach and the formation of a backwash bore. We employed the hodograph transformation to construct the solutions, which linearized the nonlinear shallow water equations, and identified that a bore formed at some interior point during the backwash; the signature of the inception of this event was that the hodograph transformation failed. Thereafter a discontinuous solution arose that may be viewed as a tear in the hodograph plane. Similarly to Hogg (2006) and Antuono *et al.* (2009), we were able to track the evolution of this discontinuity, however, importantly it differed from the previously studied examples in that it grew in magnitude before diminishing and finally vanishing as it intersected with the retreating shoreline. Although generated from different boundary conditions, this shares identical features with the numerical computations of Hibberd & Peregrine (1979), who studied the run-up of a uniform bore on a planar beach. These results reveal interesting dynamics that could be studied in the laboratory and they pose a challenging test for numerical routines designed to integrate the governing equations.

There are a number of interesting developments of this work that warrant further investigation. These include predictions of over-topping from truncated beaches, sediment transport, as well as an assessment of how the results might change should a more complete model of the motion be employed.

REFERENCES

Antuono, M., Hogg, A. J. & Brocchini, M. 2009 The early stages of shallow flows in an inclined flume. *J. Fluid Mech.* **633**, 285–309.

Brocchini, M. & Baldock, T. E. 2008 Recent advances in modelling swash zone dynamics: influence of surf-swash interaction on nearshore hydrodynamics and morphodynamics. *Rev. Geophys.* **46** (RG3003), 1–21.

Brocchini, M. & Dodd, N. 2008 Nonlinear shallow water equation modelling for coastal engineering. *J. Waterway Port Coast. Ocean Engng* **134**, 104–120.

Garabedian, P. R. 1986 *Partial Differential Equations*. Chelsea Publishing.

Guard, P. A. & Baldock, T. E. 2007 The influence of seaward boundary conditions on swash zone hydrodynamics. *Coast. Engng* **54**, 321–331.

HIBBERD, S. & PEREGRINE, D. H. 1979 Surf and run-up on a beach: a uniform bore. *J. Fluid Mech.* **95**, 323–345.

HOGG, A. J. 2006 Lock-release gravity currents and dam-break flows. *J. Fluid Mech.* **569**, 61–87.

HOGG, A. J. & PRITCHARD, D. 2004 The effects of drag on dam-break and other shallow inertial flows. *J. Fluid Mech.* **501**, 179–212.

KERSWELL, R. R. 2005 Dam break with Coulomb friction: a model for granular slumping? *Phys. Fluids* **17** 057101(1–16).

PEREGRINE, D. H. 1972 Equations for water waves and the approximations behind them. In *Waves on Beaches and Resulting Sediment Transport* (ed. R. Meyer), ch. 3, pp. 95–121. Academic Press.

PEREGRINE, D. H. & WILLIAMS, S. M. 2001 Swash overtopping a truncated plane beach. *J. Fluid Mech.* **440**, 391–399.

PRITCHARD, D., GUARD, P. A. & BALDOCK, T. E. 2008 An analytical model for bore-driven run-up. *J. Fluid Mech.* **610**, 183–193.

PRITCHARD, D. & HOGG, A. J. 2005 On the transport of suspended sediment by a swash event on a plane beach. *Coast. Engng* **52**, 1–23.

RITTER, A. 1892 Die Fortpflanzung der Wasserwellen. *Zeitschrift des Vereines Deutscher Ingenieure* **36** (33), 947–954.

SHEN, M. C. & MEYER, R. E. 1963 Climb of a bore on a beach. Part 3. Run-up. *J. Fluid Mech.* **16**, 113–125.

ZHANG, Q. & LIU, P. L.-F. 2008 A numerical study of swash flows generated by bores. *Coast. Engng* **55**, 1113–1134, doi:10.1016/j.coastaleng.2008.04.010.